Numerical Example

For a satellite originally in a 100-naut-mile circular orbit with a constant tangential thrust of $2.05 \times 10^{-5} g_e M_0$, the following are assumed:

$\rho_0 = 5 \times 10^{-13}$ slug ft^{-3}

$C_D A/2M_0 = 1$ ft^2 slug^{-1}

$\bar{c} = 64.4 \times 10^3$ fps

$\beta = 4.74 \times 10^{-6}$ ft^{-1}

$\gamma(a_0) = 0.945$ from Ref. 4

The results in Table 1 are obtained directly by substitutions into various equations in the analysis.

Conclusion

The approximations presented here for the spiral trajectory under the perturbations of aerodynamic drag and a low constant tangential thrust are particularly useful for preliminary estimates of propulsion requirements and in mission analyses related to low-altitude orbit around the earth. Attempts should be made to investigate low-thrust spiral trajectories as affected by aerodynamic drag, including the effects of oscillation, which may be useful for guidance design of a satellite.

References

[1] Lawden, D. F., "Optimal programming of rocket thrust direction," Astronaut. Acta. **1**, 41–56 (1955).

[2] Zee, C. H., "Trajectories of satellites under the influence of air drag," AIAA Preprint 63-392 (1963); to be published in *AIAA Progress in Astronautics and Aeronautics: Celestial Mechanics and Astrodynamics* (Academic Press, Inc., New York, 1964), Vol. 14.

[3] Zee, C. H., "Low constant tangential thrust spiral trajectories," AIAA J. **1**, 1581–1583 (1963).

[4] Melbourne, W. G., "Interplanetary trajectories and payload capabilities of advanced propulsion vehicles," Jet Propulsion Lab. TR 32-68, California Institute of Technology, Pasadena, Calif. (March 1961).

Dynamic Stability Testing in a Mach-14 Blowdown Wind Tunnel

OTTO WALCHNER,* FRANK M. SAWYER† AND STEPHEN J. KOOB‡

Aerospace Research Laboratories, Wright-Patterson Air Force Base, Ohio

Nomenclature

d = base diameter of cone model, ft
D = coefficient of structural damping moment, ft-lb-sec
I = moment of inertia with respect to pitch axis, slug-ft^2
k = flexure spring constant, ft-lb/rad
M = pitching moment, ft-lb; also Mach number
q = $(\rho/2)V^2$, dynamic pressure, psf
S = $(\pi/4)d^2$, base area, ft^2
T = absolute temperature, °R
V = freestream velocity, fps
α = variation of angle of attack from trim, rad

Received January 17, 1964; revision received April 13, 1964.

* Research Aerospace Engineer, Hypersonic Research Laboratory.

† Research Physicist, Hypersonic Research Laboratory.

‡ Research Aerospace Engineer, Fluid Dynamics Facilities Laboratory; also First Lieutenant, U. S. Air Force. Associate Member AIAA.

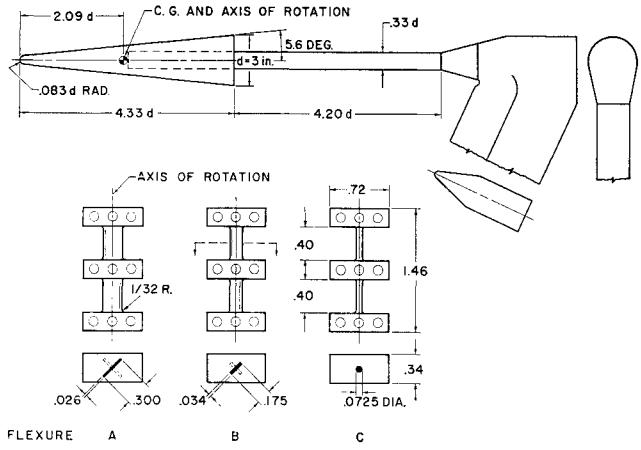

Fig. 1 Model, support system, and flexures used for dynamic stability tests; flexure dimensions in inches.

δ = logarithmic decrement
θ = variation of pitch angle from trim, rad
μ = coefficient of viscosity, slug/sec-ft
ρ = freestream density, slug/ft^3
ω = circular frequency, rad/sec
$(.)$ = derivatives with respect to time

Subscripts

1 = "wind-on" condition
2 = "wind-off" condition
t = total or isentropic stagnation condition

Definitions

C_m = M/qSd, pitching moment coefficient

C_{m_α} = $(\partial C_m/\partial\alpha)$, static stability derivative

$$C_{m_q} + C_{m_{\dot\alpha}} = \frac{\partial C_m}{\partial[(d/2)(\dot\theta/V)]} + \frac{\partial C_m}{\partial[(d/2)(\dot\alpha/V)]},$$

dynamic stability derivatives

Introduction

THE relatively long-run times of blowdown wind tunnels make this type of hypersonic test facility very attractive for dynamic stability testing. A great number of cycles of oscillation can be observed during one run, even at the lowest frequency of interest. A feasibility study for dynamic stability testing in one of the Aerospace Research Laboratories' hypersonic wind tunnels at Mach 14 is reported here. Use is made of the one-degree-of-freedom, small-amplitude, free-oscillation technique in which the model is connected to the supporting system by an elastic torsion rod (flexure). The data presented refer to zero trim angle of attack only.

Apparatus

For a description of the wind tunnel and its operation, see Refs. 1 and 2. The investigated cone model and the support system are sketched in Fig. 1, which also shows the design of three different beryllium copper flexures. The middle block of the flexure is connected to the stationary sting, and the outer blocks are connected with a mount carrying the model. It is not uncommon in this type of hypersonic testing that the energy dissipation by structural damping moments exceeds the aerodynamic damping by an order of magnitude. The design of the flexures shown in Fig. 1 was intended to reduce the structural damping to a lower level than is usually experienced. The spring constants of 9.10, 7.99, and 8.21 ft-lb/rad were found by static calibration of the flexures A, B, and C, respectively. No change of these values was experienced when an additional load was applied to simulate the effects of a steady lift or drag force. The flexures A and B have the advantage over C of greater structural rigidity in all

Table 1 Test data compiled from seven runs with three different flexures at zero trim angle

Test no.	Stagnation conditions		Reduced frequency, $(d/2)(\omega_1/V)$	Reynolds no., $Vd\rho/\mu \times 10^{-6}$	Stability derivatives	
	p_t, psi	T_t, °R			$Cm_q + Cm_{\dot\alpha}$	Cm_α
1[a]	1414	2120	0.0014	0.13	−1.81	−1.13
2[b]	1714	2030	0.0013	0.17	−1.77	−1.12
3[b]	1714	2020	0.0013	0.17	−1.86	−1.10
4[b]	1714	2080	0.0013	0.16	−1.80	−1.13
5[c]	1414	1940	0.0014	0.15	−1.68	−1.15
6[c]	1414	1890	0.0014	0.175	−1.68	−1.09
7[c]	1714	1880	0.0014	0.195	−1.86	−1.05

[a] Wide-strip flexure, A.
[b] Narrow-strip flexure, B.
[c] Circular-rod flexure, C.

other degrees of freedom than the intended pitch. Flexure C excels by a very low structural damping and by a wider angular range for which the spring moment varies linearly with the displacement.

Seven wind-tunnel runs were made at zero trim angle of attack with total pressures ranging from 1400 to 1700 psi and total temperatures from 1800° to 2100° R. The air flow in the test section is supersaturated at these conditions but not liquefied.[3, 4] Tare runs without wind were made immediately before and after each "wind-on" run, with the test cabin evacuated to 1 mm Hg. The purpose of the second "wind-off" run was to make certain that aerodynamic heating during the foregoing wind-on run did not alter the spring constant and the structural damping. For lack of better instrumentation, a high-speed motion picture camera was used to obtain the time history of the displacement amplitude and the frequency. The accuracy of the amplitudes is estimated to be within ±0.01.

Stability Derivatives

The linearized moment equation for a one-degree-of-freedom oscillation in pitch may be written

$$I\ddot{\alpha} = (M_{\dot\theta} + M_{\dot\alpha} - D_1)\dot\alpha + (M_\alpha - k)\alpha \quad \text{(wind-on)} \quad (1)$$

$$I\ddot{\alpha} = -D_2\dot\alpha - k\alpha \quad \text{(wind-off)} \quad (2)$$

For small damping moments, the solution of Eqs. (1) and (2) with constant coefficients leads to

$$D_1 - (M_{\dot\theta} + M_{\dot\alpha}) = (1/\pi)I\omega_1\delta_1 \quad (3)$$

$$k - M_\alpha = I\omega_1^2 \quad (4)$$

$$D_2 = (1/\pi)I\omega_2\delta_2 \quad (5)$$

$$k = I\omega_2^2 \quad (6)$$

In Eqs. (1) and (2), the small, actually nonlinear, structural damping moment is substituted by an equivalent viscous type of damping moment $D\dot\alpha$, and the actual deviations from the linear concept are considered as effects of frequency and amplitude on the coefficient D. Dynamic calibration with different moments of inertia indicated, in agreement with Ref. 5, that the logarithmic decrement δ_2 did not vary with frequency (flexure C) or varied only slightly (flexures A and B). It follows from Eqs. (5) and (6) that

$$D_2\omega_2 = (1/\pi)k\delta_2 = \text{const} = D_1\omega_1 \quad (7)$$

In other words, the coefficient D in Eqs. (1) and (2) varies inversely with frequency—this result was also found by other investigators for crossed beam flexures.[6]

Combining Eqs. (3–7), and using the definitions mentioned previously, it is seen that the stability derivatives become

$$C_{m_q} + C_{m_{\dot\alpha}} = -\frac{8}{\pi}\frac{d}{2}\frac{\omega_1}{V}\frac{I}{\rho Sd^3}\left[\delta_1 - \left(\frac{\omega_2}{\omega_1}\right)^2\delta_2\right] \quad (8)$$

$$C_{m_\alpha} = -8\left(\frac{d}{2}\frac{\omega_1}{V}\right)^2\frac{I}{\rho Sd^3}\left[1 - \left(\frac{\omega_2}{\omega_1}\right)^2\right] \quad (9)$$

The tests must yield the logarithmic decrement and the frequency, both for wind-on and wind-off conditions. Besides the physical model constants, S, d, and I, the freestream density and the wind velocity must be determined.

Results

Figures 2 and 3 show typical examples of the decaying amplitude vs number of cycles. Meaningful differences of the logarithmic amplitude decay between wind-on and wind-off conditions were obtained with all flexures. In all cases, both tare runs were in agreement. Fairly repeatable derivatives were obtained with different flexures and at slightly different tunnel conditions (Table 1). The negative values of both derivatives indicate that this particular model is statically and dynamically stable at zero trim angle of attack.

In fair agreement with the observed static derivatives is the value $C_{m_\alpha} = -1.06$, derived from the blunted cone correlation data presented in Ref. 7. This value may be in error by approximately ±7% because of the scatter of the normal force coefficients for $\alpha \to 0$ (Fig. 2 in Ref. 7). The Newtonian impact theory with a pressure coefficient of 2.0 for a surface normal to the flow direction predicts $C_{m_\alpha} = -1.23$, which also seems to agree fairly well with the oscillation tests. However, this agreement may be accidental, since the impact theory is not applicable on the surface of a blunted slender cone downstream of the nose. There are no data in the open literature known to the authors for a comparison with the observed dynamic derivatives. The impact theory predicts, for the model investigated, $C_{m_q} = -6.8$, which is four times the experimental value. If good agreement with the impact theory is reported by other investigators, the data always refer to larger cone angles, to pointed cones, or to larger amplitudes and different frequencies, e.g., Ref. 8.

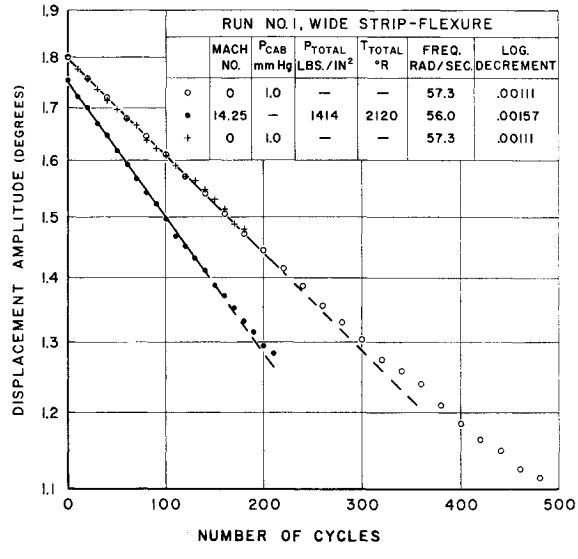

Fig. 2 Amplitude decay of cone model mounted to flexure A.

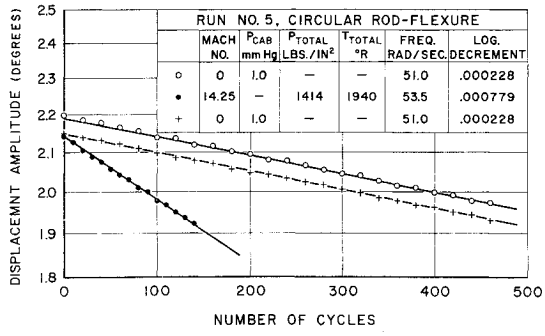

Fig. 3 Amplitude decay of cone model mounted to flexure C.

The reason for the obviously low damping derivatives will be investigated further. It is intended to investigate the effects of nose bluntness, oscillation amplitudes, and frequencies on the damping. A quasi-steady analysis is planned, based on the experimentally determined normal force distribution along the model. The investigation will be extended to various trim angles of attack.

References

[1] Gregorek, G. M. and Lee, J. D., "Design performance and operational characteristics of the ARL twenty-inch hypersonic wind tunnel," Aerospace Research Labs. Rept. 62-392 (1962).

[2] Gregorek, G. M., "Initial calibration and performance of the ARL twenty-inch hypersonic wind tunnel," Aerospace Research Labs. Rept. 62-393 (1962).

[3] Daum, F. L., "Air condensation in a hypersonic wind tunnel," AIAA J. **1**, 1043–1046 (May 1963).

[4] Goddard, R., "Liquefaction tests in the ARL twenty-inch hypersonic wind tunnel," unpublished data (1963).

[5] Gemant, A., *Frictional Phenomena* (Chemical Publishing Co., Inc., New York, 1950), Chap. XVI, p. 328.

[6] Welsh, C. J. and Ward, L. K., "Structural damping in dynamic stability testing," Arnold Engineering Development Center TR 59-5 (1959).

[7] Whitfield, J. D. and Wolny, W., "Hypersonic static stability of blunt slender cones," Arnold Engineering Development Center TDR 62-166 (1962).

[8] Jaffee, P., Preslin, R. H., and Dayman, B., *Space Programs Summary*, JPL Rept. 37-24 (Jet Propulsion Laboratories, California Institute of Technology, Pasadena, Calif., 1963), Vol. IV, pp. 72–78.

Approximate Payload Capabilities of Boosters for Planetary Missions

ALAN B. BAKER*
Radio Corporation of America, Princeton, N. J.

Nomenclature

E = injection energy, joules
g = gravitational constant, 9.81 m/sec²
I_{spj} = specific impulse of the jth stage, sec
m_1 = escape mass, kg
n = number of booster stages
P = weight of payload, lb
R = radius of Earth, 6.38 (10^6) m
r_0 = parking orbit radius, 6.57(10^6) m
W_{ij} = weight of vehicle at beginning of jth stage, lb
W_{fj} = weight of vehicle at end of jth stage, lb
V = actual terminal velocity at injection, m/sec
V_L = velocity loss because of drag and gravity, 1524 m/sec (5 kft/sec)

Received March 4, 1964; revision received April 8, 1964.
* Associate Engineer, Astro-Electronics Division.

THE payload capability of any chemical booster depends primarily on its ascent trajectory and the injection energy required for the particular mission. At the end of the ascent phase, the spacecraft must have a final velocity and orientation to permit escape from the earth's gravitational field and to rendezvous, at the proper time and place, with the target planet. There are two alternative ascent paths: a direct-ascent trajectory, where the booster stages burn successively, with only short coast periods to permit separation of the stages; and a parking-orbit trajectory, where the burning time is divided into two periods, separated by a coasting interval in a circular orbit. The parking-orbit trajectory is much preferred to the direct ascent, although the latter has shorter flight time.[2] The major disadvantage of the latter is that it must satisfy both the energy requirements and the geometrical constraints simultaneously, which results in a narrow launch window, an inefficient ascent path, and a loss in payload capability. Parking orbit trajectories permit higher payloads and more flexibility in launching time because the in-orbit time and launch azimuth can be varied for the same mission. The lowest possible parking-orbit altitude permits the greatest payload capability, and this capability decreases as the altitude is increased. A 100-naut-mile parking orbit ascent trajectory was assumed in all calculations.

The optimum type-I transfer characteristics for the planets under consideration are listed in Table 1, abstracted from Clarke's tables.[1] These optimum conditions are cyclic and each occurs once during the planet's metonic cycle.† Mars' metonic cycle is 15 yr. The characteristics for the period listed for Mars will repeat for the period 1977 through 1992. No transfer characteristics are listed for Venus beyond 1970, since its metonic cycle is ~8 yr; the conditions listed will repeat for the period 1970 through 1978 and again during 1978 through 1986. Jupiter's metonic cycle is ~12 yr, but because of its nearly circular orbit and relatively large distance from Earth, there is very little variation in these characteristics from year to year—the required geocentric injection energy ranges from 0.77(10^8) to 1.1(10^8)m²/sec² for 1968 through 1973, and launch windows occur every 13 months. Mercury's metonic cycle is ~1 yr; hence, the conditions shown occur annually.

Geocentric injection energy is the vehicle's remaining kinetic energy after it escapes from the Earth's gravitational field. It is independent of the heliocentric flight path and is defined by the equation

$$E = \tfrac{1}{2}m_1V^2 - gR^2m_1/r_0 \quad (1)$$

or

$$2E/m_1 = V^2 - 1.216(10^8) \quad (2)$$

Values of $2E/m_1$ are tabulated in Table 1.

It is theoretically possible to travel from Earth to a planet on several different ballistic paths at any given moment, but only a small number of these paths have a sufficiently low injection energy requirement to be usable with currently available or planned boosters. Of these, the most practical paths are those that require less than one revolution about the sun. Type I trajectories make less than one-half of one revolution about the sun and type II trajectories make between one-half and one revolution around the sun. Within each type there are two possible trajectories, class I and class II. Class I has a smaller heliocentric central angle and hence a shorter flight time than class II.[3]

The value of $2E/m_1$ listed in Table 1 for a particular launch period is the greatest value that might be required to launch the vehicle at any time within that period. The launch date requiring the minimum energy occurs at some time within the smallest launch interval. These listings show that a

† The period of cyclic occurrence of the same absolute fixed geometry between Earth and the planet. The length of this cycle depends on the planet's orbital velocity relative to Earth.